

MECHANICAL CHARACTERIZATION OF STEEL FOR FASTENING
IN A WIDE RANGE OF STRAIN RATE

E. C a d o n i¹⁾, A. M. B r a g o v²⁾, M. D o t t a¹⁾, D. F o r n i¹⁾,
A. K o n s t a n t i n o v²⁾, A. L o m u n o v²⁾, A. R i p a m o n t i³⁾

¹⁾ **University of Applied Sciences of Southern Switzerland**
DynaMat Laboratory
Switzerland

²⁾ **State University of Nizhny Novgorod**
Research Institute of Mechanics
Russia

³⁾ **Agrati Group S.p.A.**
Italy

In this paper, the preliminary results of the mechanical characterization in a wide range of strain rate of the 30MnB4 steel, usually adopted for fasteners, are described. In this study the different issues required to implement the dynamic test results in numerical code have been analyzed. Different experimental techniques have been used for different strain rates: universal machine, Hydro-Pneumatic Machine, JRC-Modified Hopkinson Bar and Split Hopkinson Pressure Bar. The failure at high strain rate has been examined by means of fast digital image recording systems. The material shows enhanced mechanical properties increasing the strain rate: this fact can be taken into consideration to improve the product design and the manufacturing process. The experimental research has been developed in the DynaMat laboratory of the University of Applied Sciences of Southern Switzerland and in the Laboratory of Dynamic Investigation of Materials in Nizhny Novgorod, in the frame of the Swiss – Russian Joint Research Program.

1. INTRODUCTION

The fastening technology is of capital importance in the transport fields (aeronautic, automotive, etc.). Thanks to the development of advanced modeling tools, as FE codes, it is now possible to study the manufacturing process of fasteners, which are, for some aspects, similar to impacts (forming loads are applied in fraction of seconds). Such advanced modeling tools require information about the strain rates behavior of materials in terms of constitutive laws in a large range of strain rates. The experimental research developed by the

DynaMat laboratory of the University of Applied Sciences of Southern Switzerland in collaboration with Agrati Group, is inserted in this frame. The paper describes experimental techniques used to carry out dynamic tensile tests on steels used in fastening. The high strain rate tests have been performed using a JRC-Modified Hopkinson Bar (JRC-MHB) and a Split Hopkinson Pressure Bar (SHPB), while the medium strain rate tests have been performed by means of a Hydro-Pneumatic Machine (HPM). The tests have been carried out loading the specimens with tensile stress at different strain rates, from 5 to 2500 1/s.

The analysis of the material has been carried out studying both the experimental results in terms of engineering and true stress versus strain curves and fracture. The characteristics of fracture, the reduction of area of the specimen cross-section after failure in the necking zone, as well as the fracture strain, have been obtained by means of acquisition of two images, before and after the failure of the specimen. The tests have been also filmed utilizing a high speed camera in order to obtain information about the progression of the necking phase.

The higher strain rate tests have been carried out in the Laboratory of Dynamic Investigation of Materials in Nizhny Novgorod, in the frame of the Swiss – Russian Joint Research Program.

1.1. Manufacturing process

The production of a bolt for fastening is a quite complex process including wire/rod preparation, cold, warm or hot forming and thread rolling. A typical rod preparation cycle consists in: annealing of steel coils (spheroidizing); pickling in H_2SO_4 ; phosphating; cold drawing; storage before cold forming.

Fasteners are usually produced in multi-station forming machines, by cutting, heading and extrusion of the material, and thread rolling. The speed of these operations are rather high, in fact a multi-station forming machine is normally able to produce 60 to 200 pieces by minute, according to the fastener dimension and complexity.

After the forming process, the cycle usually includes heat treatment to give the defined mechanical properties, and the application of coating/lubrication on fasteners, to ensure performances in terms of corrosion resistance and friction coefficient. The result of a finite element analysis of the cold forming cycle is shown in Fig. 1. In this example, the total equivalent plastic strain is the selected parameter.

All four cold forming steps are shown in Fig. 2. The last but one is the result of thread rolling; and the last one in the picture is the bolt after heat treatment and after non-electrolytically applied zinc flake coating. Thread is obtained by plastic deformation of the shank, without any removal of the material.

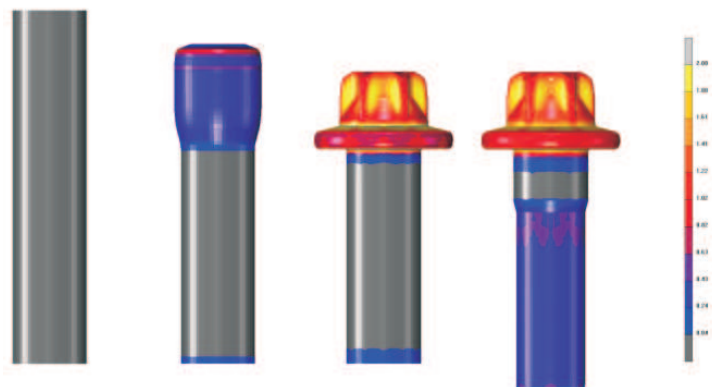


FIG. 1. FEM results of the cold forming cycle.



FIG. 2. Sequence of cold forming of fastener.

2. MATERIAL

The analyzed material is the 30MnB4 steel, according to EN 10263-4 [1]. The chemical composition of this steel is shown in Table 1.

Table 1. Chemical composition.

	C	Si	Mn	P	S	Cr	Mo	Cu	B
Standard Requirements	0.27÷0.32	≤ 0.30	0.80÷1.10	≤ 0.025	≤ 0.025	≤ 0.30	–	≤ 0.25	0.0008÷0.005
Specimens	0.28	0.12	0.83	0.01	0.004	0.17	–	0.13	0.0027

The steel was supplied by the steelmaker in hot-rolled condition, with rod diameter of 7.50 mm. The material is normally characterized by a tensile strength $R_m = 632 \div 640$ MPa and the percentage reduction of area after fracture $Z = 62 \div 50\%$.

In this case, after the preparation cycle, the rod for specimens has got the following characteristics:

- diameter = 6.15 mm (reduction of area during cold drawing $\approx 33\%$);
- tensile strength $R_m = 695 \div 720$ MPa;
- percentage reduction of area after fracture $Z = 55 \div 59\%$;
- core hardness ≈ 238 HV_{0.3}.

The micro-hardness scanning (Fig. 3) shows superimposed effects of hot rolling, annealing and cold drawing processes of the rod.

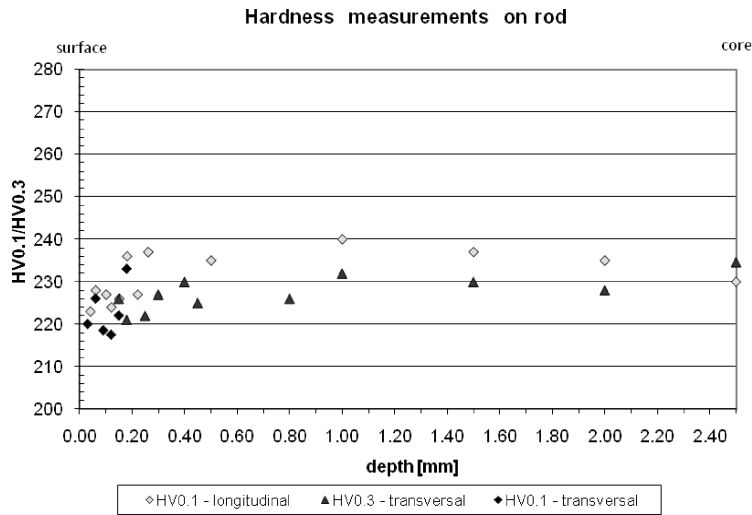


FIG. 3. Hardness distribution on the depth.

To discuss micro-hardness profiles it is important to take into consideration the residual stresses distribution, whose effects are to be added to the grain dimensions.

In Fig. 4a and Fig. 4b the transversal and the longitudinal section in the core are shown ($500\times$). In the first picture it is possible to observe the not completely

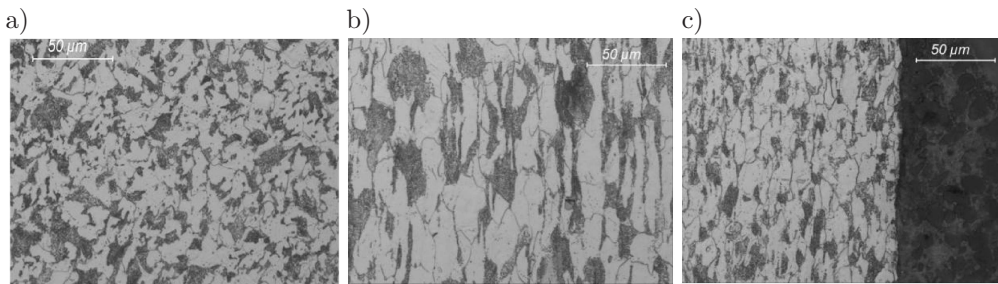


FIG. 4. Ferritic-pearlitic micro-structure.

lamellar pearlite and in the second picture – the longitudinal “pancaked” grain. Finally, in Fig. 4c, the longitudinal section at the surface ($500\times$) is shown, where the grain refinement compared to the core micro-structure is evident.

3. EXPERIMENTAL PROGRAM

The experimental techniques for high-strain-rate measurements are described in literature [2–7]. The dynamic tests were conducted on round specimens depicted in Fig. 5.

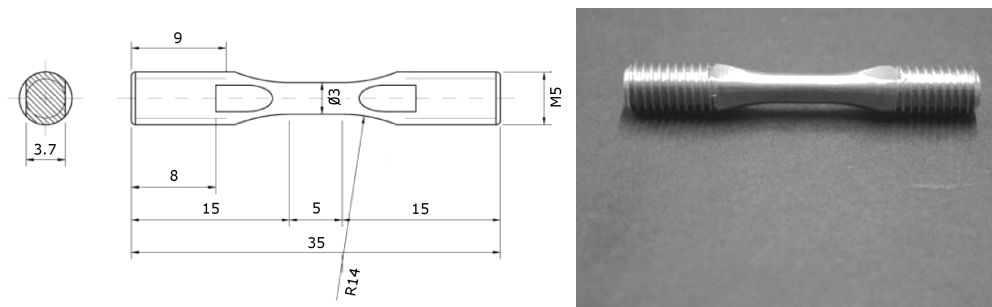


FIG. 5. Specimen geometry.

These specimens were tested in different conditions: using stroke-controlled static procedures and with HPM, JRC-MHB and SHPB dynamic experimental techniques. The Universal Machine used for quasi-static tests and the HPM used for medium strain rates are shown in Fig. 6.

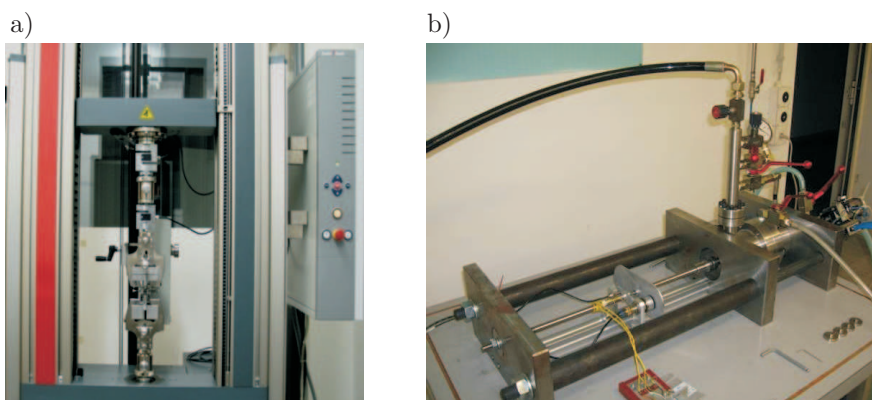


FIG. 6. a) Universal Machine; b) Hydro-Pneumatic Machine.

The JRC-MHB has been used for high strain-rate tests and consists of two cylindrical high strength steel bars, having a diameter of 10 mm, with length

of respectively 9 and 6 m for the input and output bar. The steel specimen is assembled between the two bars, as shown in Fig. 7 [8–9].

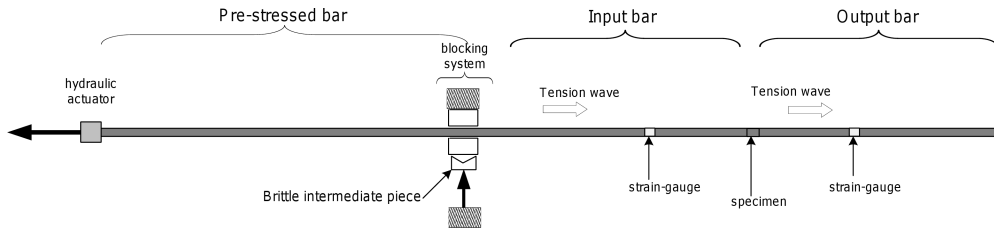


FIG. 7. JRC-MHB scheme.

The test with the MHB is performed as follows:

- 1) an hydraulic actuator, with maximum loading capacity of 600 kN, applies a tensile load on a part of the input bar (pre-stressed bar, with a length of 6 m and diameter of 10 mm); a blocking device permits to store elastic energy pulling the pre-tension bar;
- 2) breaking of the brittle bolt in the blocking device gives rise to a tensile mechanical pulse, which propagates along the input and output bars and brings the specimen to fracture. The pulse has a duration of 2.4 ms, with linear loading rate rise time of 30 μ s.

The input and output bars are instrumented with strain gauges which measure the incident, reflected and transmitted pulses acting on the cross-section of the specimen. A part of the input bar is used as a pre-stressed bar. On the basis of the incident (ε_I), reflected (ε_R) and transmitted (ε_T) records, of the consideration of the basic constitutive equation of the input and output elastic bar material, of the one-dimensional wave propagation theory, it is possible to calculate the stress, strain and strain-rate curves with the following equations [10–12]:

$$(3.1) \quad \sigma_E(t) = E_0 \frac{A_0}{A} \varepsilon_T(t), \quad \varepsilon_E(t) = -\frac{2C_0}{L} \int_0^t \varepsilon_R(t) dt, \quad \dot{\varepsilon}(t) = -\frac{2C_0}{L} \varepsilon_R(t),$$

where E_0 is the elastic modulus of the bars; A_0 is their cross-section area; A is the specimen cross-section area; L is the specimen gauge length; C_0 is the sound velocity of the bar material.

Similar tests have been carried out using a traditional SHPB (Fig. 8) placed in the Nizhny Novgorod State University [13]. Pulse loads in a SHPB are generated using compact 10-mm gas guns. Tensile tests are conducted following the modified Nicholas scheme [14]. For testing high-strength steel, pressure bars of 12 mm diameter were used. The first pressure bar is 1.5 m long and the second

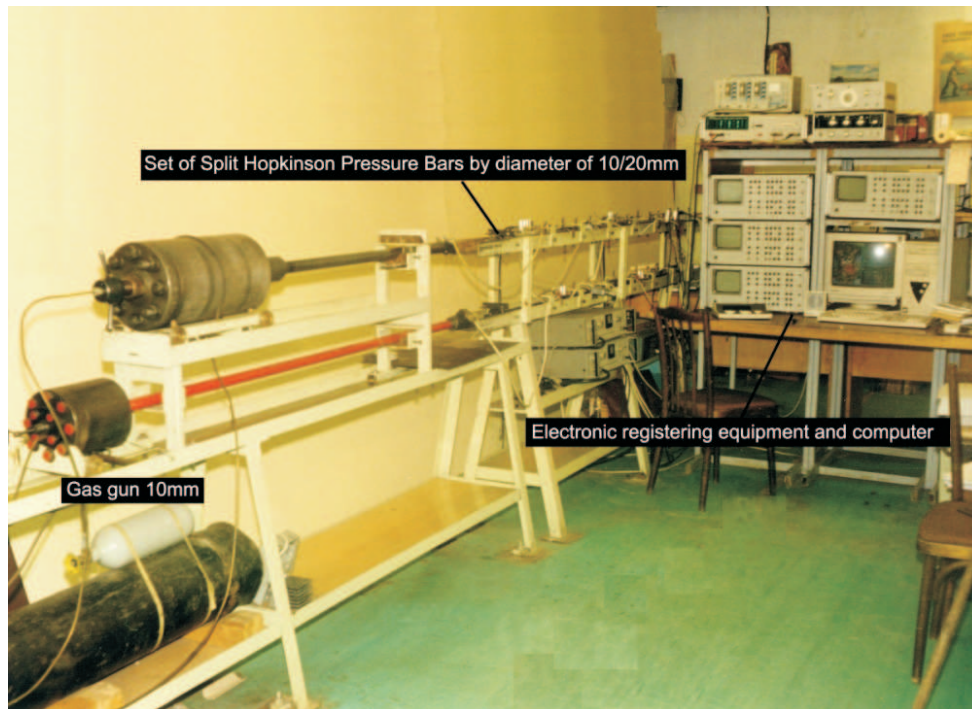


FIG. 8. SHPB for dynamic tests.

bar that has a free rear end is 0.75 m long. Tensile pulse in the Nicholas' scheme is formed due to the presence of a split ring surrounding the specimen (Fig. 9) and reflection of the transmitted pulse from the free rear end of the second bar.



FIG. 9. Phases of the assembly of the specimen to the testing device.

4. RESULTS AND DISCUSSION

The results of the preliminary tests are collected in Table 2. In Fig. 10 the engineering and true stress versus strain are depicted.

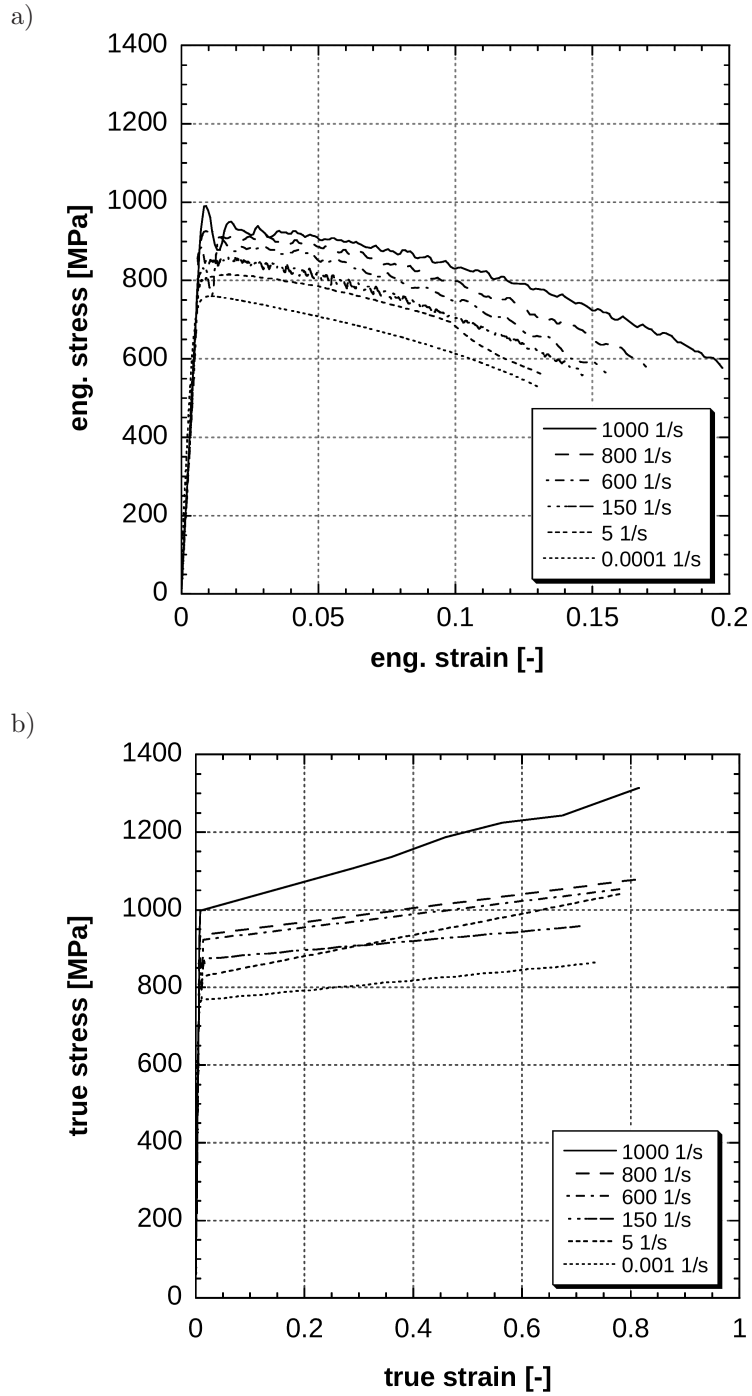


FIG. 10. a) engineering stress vs. engineering strain curves; b) true stress vs. true strain curves.

Table 2. Experimental results.

Strain rate [s ⁻¹]	R_m [MPa]	Uniform elongation ε_u	Total elongation ε_t	Reduction of area Z [%]
10 ⁻³	770	1.2%	13.1 %	52.3
5	815	1.7%	13.2%	52.4
150	856	1.7%	14.6%	50.6
600	899	1.4%	15.5%	54.5
800	926	1.0%	16.9%	55.7
1000	990	0.9%	19.7%	55.7

In order to analyze the failure behavior of 30MnB4 steel, some tests have been recorded by a Specialized Imaging Duplex Ultra Fast Framing Camera (with a speed up to 200 Mfps, see Fig. 11b), able to record up to 16 images without compromising on shading, or parallaxing. In Fig. 11a is shown the engineering stress versus strain curves, with the indication of the photo made by the fast camera.

The photos of the failure (Fig. 11c-h) reveal the ability of the camera to capture the necking process.

The true stress vs. true strain curve is regarded as significant until the ultimate tensile stress (where the necking begins) is reached. After this point, stress localization and fracture propagation governs the flow curve, which is no more representative for homogeneous mechanical properties of the materials. In this case, beyond the point of ultimate strength in the engineering stress-strain curve, the one-dimensional true stress-strain curve should be reconstructed, by calculating the true stress and the true strain using the Bridgman formulae, [15] which introduces the correction for the triaxial stress state. At fracture the Bridgman formulae can be written as follows:

$$(4.1) \quad \sigma_{\text{true,fracture}} = \frac{\sigma_{\text{eng.,fracture}}}{(1 + 2R/a) \cdot \ln(1 + a/2R)},$$

where a – minimum radius at fracture cross-section, R – meridional profile radius at fracture neck (see Fig. 13a), $\sigma_{\text{true,fracture}} = P_{\text{fracture}}/\pi a^2$ – the average true stress at fracture and P_{fracture} the fracture force.

$$(4.2) \quad \varepsilon_{\text{true,fracture}} = 2 \cdot \ln \frac{a_0}{2 \cdot a},$$

where a_0 is the initial diameter of the gauge length cross-section.

For the complete construction of the true stress-strain curve during the necking deformation phase, a straight line is drawn between the ultimate tensile strength (uniform strain) point and the fracture point, the latter being determined by application of Eqs. (4.1) and (4.2).

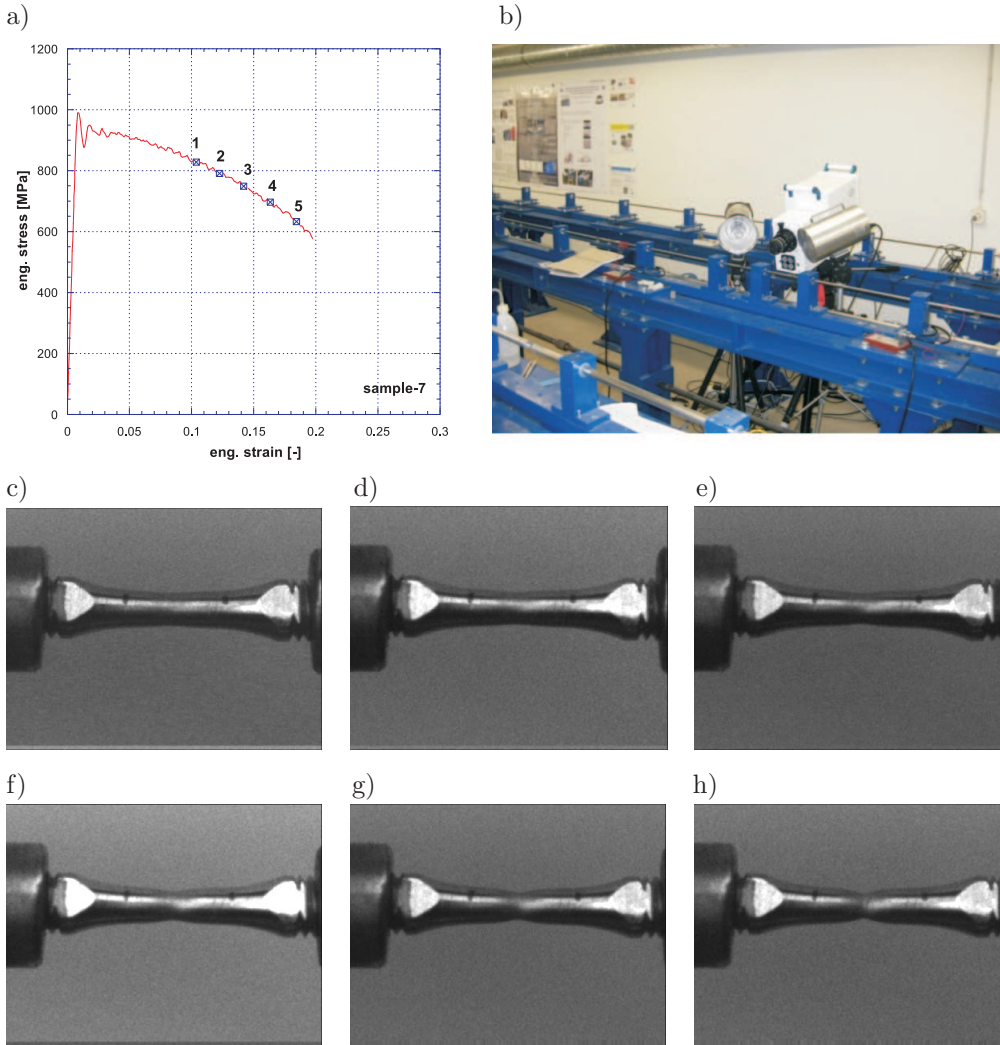


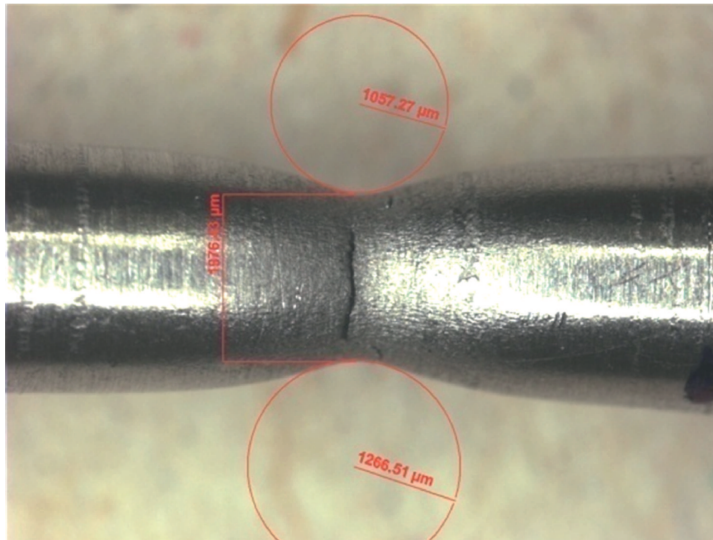
FIG. 11. High speed digital camera.

A more refined determination of the true stress vs. true strain curve between the point of ultimate tensile strength (uniform strain) and the point of fracture, has been performed, using the following method:

- fast recording of the test,
- repetition, at defined increasing deformation levels, of the optical measurements of the meridional radius at neck (R) and of the minimum radius at neck cross-section (a),
- calculation, with the Eqs. (4.1) and (4.2), of the true stress and true strain values, for the defined deformation levels.

In Fig. 12b the results of the described measurement are shown. It is possible to observe how well the linear trend describes the necking process in the true stress vs. true strain diagram. Subsequently we have demonstrated a good approximation of the procedure which only exploits the Bridgman formulae and the information given by the engineering curve, and by the measurement of the fracture geometry.

a)



b)

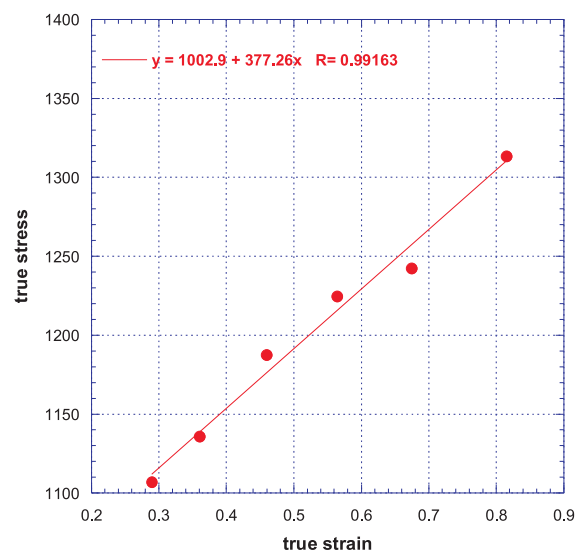


FIG. 12. a) parameter for Bridgman formulae; b) points measured by fast camera.

4.1. Comparison between JRC-MHB and SHPB

The SHPB is not able to generate enough energy to break the specimen for strain rates less than 1000 1/s because of the short length of the striker bar. The comparison of two tests performed with SHPB and JRC-MHB is shown in Fig. 13a; in the first case, the specimen is only deformed to the necking phase (see Fig. 13b) while in the JRC-MHB all the plastic fields are detected, till failure. At the moment, the JRC-MHB set up does not reach the same velocities of the SHPB. To obtain those values, the JRC-MHB should be realized in very high strength material (for instance a thermally aged, maraging steel), instead of the high strength steel actually utilized. In order to obtain low strain rate with the SHPB, longer striker bar should be adopted.

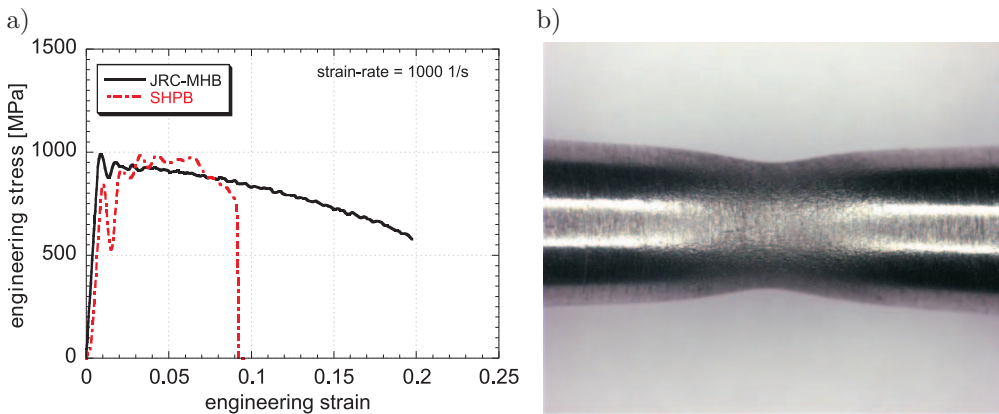


FIG. 13. a) Comparison of the two test set-ups; b) Necking in the specimen.

During the testing activities, the influence of the rise time of the load process on the materials behavior, in the elastic range, has been noted. This phenomenon, observed for HSS steels, is evidenced as an instability of the curves, which shows a high first peak. The rise time of the SHPB set-up is about 150 μ s, while the JRC-MHB set-up reaches up to 30 μ s.

For the tensile tests in particular, the JRC-MHB set-up permits to obtain a perfect direct loading of the specimen, while in the SHPB set-up this is obtained by inversion of the waves at the free end of the bar. The comparison between the records observed within the two solutions is shown in Fig. 14.

Specimens at high strain rates, over 1000 1/s, have been tested with the SHPB apparatus.

Three true stress curves versus true strain curves are depicted in Fig. 15a. The increase of the ultimate tensile strength in function of the logarithm of the strain rate is shown in Fig. 15b. Up to 1000 1/s, the Dynamic Increase Factor is less than 1.2; for higher true strain values the DIF could be more than 1.8.

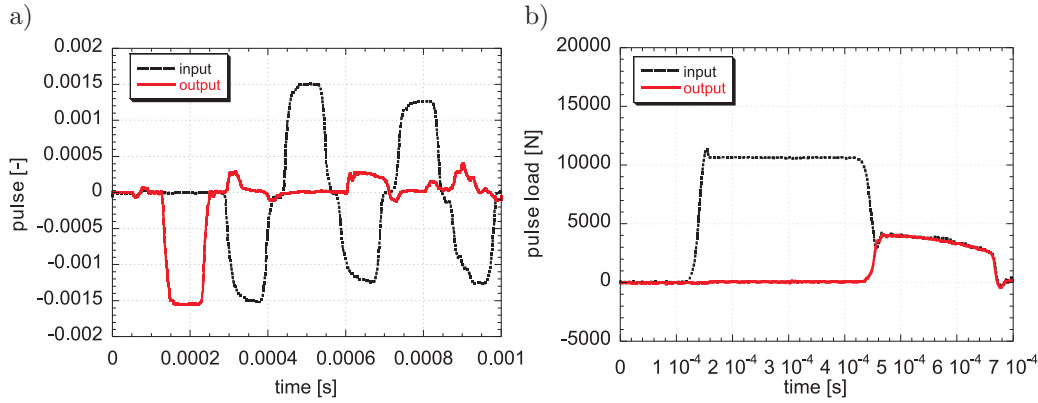


FIG. 14. Signals from: a) SHPB; b) JRC-MHB.

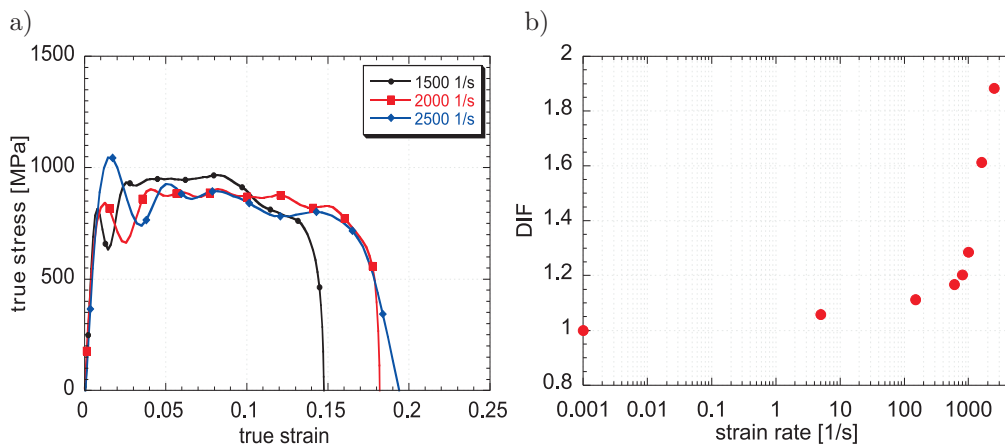


FIG. 15. a) high strain rate tests with SHPB; b) Dynamic Increase Factor (DIF) versus strain rate.

5. EXAMPLE OF A MATERIAL CONSTITUTIVE LAW CALIBRATION

Advanced modeling tools require information about the strain rate behavior of materials in terms of constitutive laws in a large range of strain rates. Also in the case of fasteners this topic cannot be avoided. In this paragraph the plastic behavior of the 30MnB4 steel by the Johnson-Cook constitutive model [16] is explained. This model is intensively used to describe the material strength in the numerical simulations of dynamic events and provides satisfactory results, when strain rates are lower than 10^3 s^{-1} . This model assumes that the dependence of the stress on the strain, strain rate and temperature can be multiplicatively

decomposed into three separate functions. Then, this model gives the following relation for the flow stress σ_0 :

$$(5.1) \quad \sigma_0 = [A + B \cdot (\epsilon_p)^n] \cdot \left[1 + C \cdot \ln \left(\frac{\dot{\epsilon}_p}{\dot{\epsilon}_0} \right) \right] \cdot [1 - T^{*m}],$$

where ϵ_p is the equivalent plastic strain, $\dot{\epsilon}_p$ is the considered test strain rate, $\dot{\epsilon}_0$ is a reference strain rate (usually equal to 1 s^{-1}), A , B , C , n and m are five material constants that have to be determined. The parameter n takes into account the strain hardening effect, the parameter m models the thermal softening, and C represents the strain rate sensitivity. Finally T^* is:

$$(5.2) \quad T^* = \begin{cases} 0 & \text{for } T \leq T_r, \\ \frac{T - T_r}{T_m - T_r} & \text{for } T_r < T \leq T_m, \\ 1 & \text{for } T > T_m, \end{cases}$$

where T is the current temperature, T_m is the melting temperature (assumed 1507°C for the 30MnB4 steel), and T_r is a reference temperature.

5.1. Determination of A , B and n in the JC model

The experimental quasi-static data can be used to plot the plastic curve characteristic of the material at room temperature (20°C): σ_{true} versus ϵ_p . This curve is best fitted by:

$$(5.3) \quad \sigma_0 = A + B \cdot \epsilon_p^n,$$

where $A = 625 \text{ MPa}$ is the stress yield point of the static curve, while B and n are determined using a regression-analysis procedure. The obtained parameters are $B = 628.9 \text{ MPa}$ and $n = 0.4097$ (with $R^2 = 0.7672$).

5.2. Determination of C in the JC model

Firstly, it is assumed that the reference strain rate is $\dot{\epsilon}_0 = 1 \text{ s}^{-1}$. It is further assumed that the specimen remains at room temperature, thus neglecting the thermo-plastic effects ($T^8 = 0$). Assuming that the strain rate is constant during the experiment, the parameter C is evaluated for three different strain rates ($\dot{\epsilon}_p$): 5 s^{-1} , 135 s^{-1} and 611 s^{-1} .

Under these assumptions the experimental stress versus plastic strain curves were fitted with the following formula:

$$(5.4) \quad \sigma_0 = [625 + 628.9 \cdot (\epsilon_p)^{0.4097}] \cdot \left[1 + C \cdot \ln \left(\frac{\dot{\epsilon}_p}{\dot{\epsilon}_0} \right) \right].$$

5.3. Determination of m in the JC model

In order to determine the parameter m , experimental results at both the room temperature and higher temperature are needed. Experimental results at high strain rates at 20°C and 450°C have been used.

The ratio R between the stresses at a specific plastic strain can be calculated if experiments at the same strain rate are carried out. In particular, m can be evaluated as:

$$(5.5) \quad m = \frac{\log(1 - R)}{\log(T^*)}.$$

Considering the true stresses at the temperature 450°C divided by the true stresses at room temperature (20°C), in the flow true stress versus plastic strain curve, it results an average value of $R = 0.6031$. Substituting this value into Eq. (5.5), $m = 0.7448$ is obtained.

The results of the calculated parameters are reported by the following table. Figure 16 shows the goodness of the Johnson-Cook fit up to 10 1/s. For higher values of strain rates it seems that this relationship does not appropriately describe the real behavior of the material; for this reason, our attention will be focused to the development of future new constitutive laws.

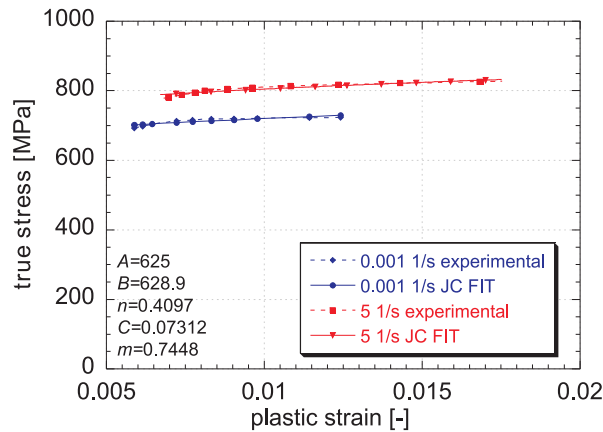


FIG. 16. Experimental data vs. JC FIT for 30MnB4 at 5 s⁻¹.

6. CONCLUDING REMARKS

The 30MnB4 steel tested in this preliminary phase resulted to be rate sensitive. This steel is usually adopted for fasteners. The manufactory process induces into the material a very complicated history of strain, provoked by cold forming and thread rolling. The production procedure is often carried out at a high

velocity, then a mechanical characterization in a wide range of strain rates is needed.

In this preliminary phase a series of tests by means of different experimental techniques have been performed, in order to show the capability of describing the actual material behavior.

It has been demonstrated how the fast recording of the failure process is well described by a linear function between the ultimate tensile strength/uniform strain, the failure point obtained by the Bridgman formulae and the geometric information by the high speed digital camera.

The high strain rate behavior has been studied by means of two types of set-ups. The traditional SHPB and the JRC-MHB have been compared. From this comparison, some comments can be summarized. First of all, the capacity of the JRC-MHB to follow the full plastic field in the range of strain rates between 100 and 1000 1/s, in the case of traditional SHPB, this is not possible without the use of longer striker bar. The JRC-MHB performs direct tensile test; the same cannot be affirmed for the SHPB. In fact, it uses the reflected wave from the free end but the presence of spurious reflection, due to the split ring, causes overlapping waves what is often difficult to analyze. The SHPB should be used in compression; to obtain direct tensile test, the pulse should be directly applied.

An example of calibration of the Johnson-Cook model has been carried out, in order to integrate the results in numerical codes and to reproduce plastic deformation occurring in dynamic regime for 30MnB4 steel.

These results indicate the advantage of using a dynamic characterization of steel, in order to improve the quality of the fastener products and enhance the production capacity.

ACKNOWLEDGEMENTS

The Authors are grateful to Mr. Wai Chan and Mr. Peter Berkenberg from “Specialised Imaging” for their precious collaboration in the execution of high speed measurements. A special acknowledgement goes to the Scientific & Technological Cooperation Programme Switzerland-Russia for the financial support of the Utilization of Specific Infrastructure Projects called “Dynamic behaviour of materials for industrial applications”. Russian part of investigations was partially financed by RFBR (grant 10-01-00585).

REFERENCES

1. EN 10263-4: 2003. “Steel rod, bars and wire for cold heading and cold extrusion. Part 4: technical delivery conditions for steels for quenching and tempering”.
2. M. A. MEYERS, *Dynamic Behavior of Materials*, Wiley Interscience, New York, 1994.

3. J. E. FIELD, *Review of experimental techniques for high rate deformation and shock studies*, Int. J. Imp. Eng., **30**, 725–775, 2004.
4. G. T. GRAY III, *Classic Split-Hopkinson pressure bar testing*, [in:] ASM Handbook, Vol. 8, H. KUHN, D. MEDLIN [Eds.], ASM Int., Materials Park Ohio 2000, pp. 462–476.
5. K. A. HARTLEY, J. DUFFY, R. H. HAWLEY, *The torsional Kolsky (Split-Hopkinson) bar*, [in:] ASM Handbook, Vol. 8, H. KUHN, D. MEDLIN [Eds.], ASM Int., Materials Park Ohio 1985, pp. 218–228.
6. S. VAYNMAN, M. E. FINE, S. LEEB, H. D. ESPINOSA, *Effect of strain rate and temperature on mechanical properties and fracture mode of high strength precipitation hardened ferritic steels*, Scripta Materialia, **55**, 351–354, 2006.
7. T. NICHOLAS, A. M. RAJENDRAN, *Material characterization at high strain-rates*, [in:] High Velocity Impact Dynamics, J.A. ZUKAS [Ed.], Wiley, New York 1990, pp. 127–296.
8. C. ALBERTINI, M. MONTAGNANI, *Testing techniques based on the split Hopkinson bar*, Institute of Physics Conference series No. 21, pp. 22–32, London, 1974.
9. C. ALBERTINI, M. MONTAGNANI, *Waves propagation effects on dynamic loading*, Journal NED 37, pp. 115–124, North Holland Publishing Company, 1976.
10. R. M. DAVIS, *A critical study of the Hopkinson bar*, Cambridge University Press, **240**, 375–457, 1948.
11. H. KOLSKY, *An investigation of the mechanical properties of materials at very high rates of loading*, Proc. Phys. Soc. Sect. **B62**, 676–700, 1949.
12. U. S. LINDHOLM, *High strain rate tests*, Techniques of metal research, J. WILEY [Ed.], **5**, 1, 1971.
13. A. M. BRAGOV, P. V. DEMENKO, A. K. LOMUNOV, I. V. SERGEICHEV, L. KRUSZKA, *Investigation of behaviour of materials of different physical nature using the Kolsky method and its modifications*, New Experimental Methods in Material Dynamics and Impact, Trends in Mechanics of Materials, W.K. NOWACKI, J.R. KLEPACZKO [Eds.], Warsaw, 2001, pp. 337–348.
14. T. NICHOLAS, *Tensile testing of materials at high rates of strain*, Exp. Mech., **21**, 5, 177–195, 1981.
15. P. W. BRIDGMAN, *Studies in large plastic flow and fracture*, Mc Graw-Hill, 1952.
16. G. J. JOHNSON, W. H. COOK, *A constitutive model and data for metals subjected to large strains, high strain rates and high temperatures*, Proceedings of the Seventh International Symposium on Ballistics, The Hague, 1983, pp. 541–547.

Received January 11, 2011; revised version June 4, 2011.
